Inhibitive action of 2-aminobezothiazole on the deterioration of AA6061-SiC composite in 0.5M HCl medium: Experimental and theoretical analysis

Navya Prabhu[a] • Prakasha Shetty[a,b]* • Preethi Kumari[a] • Sneha Kagatikar[a]

[a]*Department of Chemistry, Manipal Institute of Technology,*
Manipal Academy of Higher Education, Manipal, Karnataka, India
[b]*Department of Chemistry, Alva's Institute of Engineering and Technology, Moodbidri, Karnataka, India*

Abstract: Electrochemical testing on AA6061-15%$_{(V)}$ SiC$_{(P)}$ composite corrosion in 0.5M HCl solution containing 2-amino benzothiazole (2-ABT) was performed. 2-ABT exhibited a good inhibition efficiency of 84% by acting as a mixed inhibitor. Polarization studies showed a considerable reduction in corrosion rate, leading to increased inhibition efficiency with a rise in 2-ABT concentration. The increase in polarization resistance with a rise in 2-ABT concentration indicates the adsorption of 2-ABT on the composite, controlling corrosion. The evaluation of thermodynamic results revealed the physisorption of 2-ABT on the composite. The adsorption of 2-ABT followed Langmuir isotherm model. The surface morphological evaluation of composite specimens before and after inhibition revealed the adsorption of 2-ABT on the composite. The results of quantum chemical calculations also confirmed the adsorption of 2-ABT.

*Corresponding author.
E-mail address: prakash.shetty@manipal.edu (Prakasha Shetty).

1. Introduction

The deterioration of metals, alloys, composites, etc., which occurs due to their interaction with the environment, is known as corrosion. The interaction may be chemical or electrochemical type leading to adverse effects like material loss, plant shutdown, oil leakage due to pipeline breakage, product contamination due to metal leaching, and environmental pollution (Revie & Uhlig, 2008). Corrosion is a spontaneous process in which metals usually undergo corrosion by returning to their stable combined form. The corrosion rate will depend on the nature of the corroding material and the aggressiveness of the medium involved. It is a slow process, but the direct and indirect losses are high. The total losses due to corrosion should include the material loss and the production loss, increased maintenance cost, etc. The total annual cost of corrosion globally was estimated to be $2.5 trillion, 3-5 percent of global GDP (Koch et al., 2016). Adopting appropriate corrosion protection practices could achieve an estimated annual savings of 375 to 875 billion USD. These reports reveal the significance of conserving metallic materials from the destructive phenomenon of corrosion. In recent years, the research and inventions in this line are gaining importance in preserving the world's material resources.

Metal-matrix composites (MMCs) are a novel type of structural material. Al alloys are the most used matrix metal because of their lightweight, environmental resistance, and favorable mechanical qualities (Sharma et al., 2022). MMCs with lower density, higher specific modulus and specific yield strength were obtained by reinforcing Al alloys with various particulate or fiber materials. They are most suitable for potential applications in the aerospace and automotive industry (Rohatgi, 1993; Singla et al., 2009). AA6061-SiC composite is one such MMC produced by reinforcing AA6061 with SiC particles. MMCs are more prone to corrosion than matrix alloys. The presence of reinforcing particles or fibers causes homogeneities on surfaces exposed to aggressive environments, which acts as active sites for matrix corrosion (Bobic et al., 2010). The hydrochloric acid solutions are used commonly as pickling agents or chemical etchants in the Al alloy composite industry. During such chemical etching processes, it will require control of the matrix metal's deterioration. The corrosion of matrix materials can be best controlled by the simplest and most economical method using inhibitors (Sanyal, 1981). Organic compounds containing heteroatoms and aromatic rings showed good corrosion inhibition activity (Shetty, 2018; Xhanari & Finšgar, 2016). 2-Amino benzothiazole (2-ABT) is one such compound having multiple heteroatoms and an aromatic ring. Hence, it is expected to show good inhibition activity. The literature survey revealed the usage of 2-ABT as an effective corrosion inhibitor of steel in 1M H_2SO4 (Danaee et al., 2015), carbon

steel (Jafari et al., 2019), and mild steel in 1M HCl (Quraishi et al., 1996). It is clear from the literature survey that 2-aminobenzothiazole has not been reported as an inhibitor for AA6061-SiC composite. 2-ABT is readily soluble in an aqueous acid medium and commercially available at a reasonable cost. This research paper describes the corrosion inhibition study of AA6061- 15 % (V) SiC (P) composite in 0.5M HCl using 2-aminobenzothiazole as an inhibitor. 2-ABT showed a good inhibition performance. The experimental results were supported by the theoretical DFT studies and surface morphological analysis.

2. Materials and methods

A specimen of the composite, AA6061-15% (v) SiC (p) (referred to her afterwards as AA-SiC composite), was used in the present study. This composite was prepared using AA6061 as the base alloy reinforced with SiC particulate (99.9% purity and 23μm size) following the stir casting method. 6061Al base alloy used has the composition: Mg (1.0 wt%); Si (0.60); Cu (0.25); Cr (0.25); and Al (97.9). An AA-SiC composite cylindrical rod was cut to the required size and embedded in epoxy resin, leaving an exposed surface at one end. The specimen's exposed surface with an area of 1cm^2 was abraded with different grades (220 -1500) emery paper and finally using a disc polisher. The abraded specimen was washed first in distilled water, then acetone rinsed and dried. The corrosive medium, 0.5M HCl used in the present work, was prepared using 35% HCl by proper dilution with distilled water and standardized by the volumetric method. 2-aminobenzothiazole (Merck) is the inhibitor used. The molecular formula of 2-animo benzothiazole is $C_7H_6N_2S$, and its chemical structure is shown in "Figure 1". Its solution in the concentration range, 0.05 to 1mM, was used.
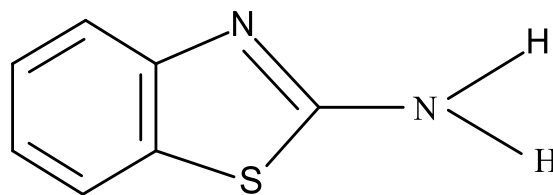

Figure 1. The structure of 2-aminobenzothiazole (2-ABT).

2.1. Electrochemical tests
The electrochemical studies were executed using a USA model CH workstation (604D series) and a cell system incorporated with a saturated calomel electrode, a reference platinum electrode, and a specimen electrode of AA-SiC composite. The exposed surface of the composite specimen was freshly

abraded and used. The cell system dipped in a corrosive medium of 0.5 M HCl was connected to the workstation. The experiment was performed at three temperatures (303, 313 and 323 K). The electrode system connected to the CH instrument was allowed to stand for about 400s to reach the steady-state condition and then recorded the open circuit potential (OCP). In the potentiodynamic polarization (PDP) technique, the working electrode polarized at a scan rate of 1mV s^{-1} between -250 mV and +250 mV. The Tafel plots were recorded. In EIS (Electrochemical impedance spectroscopy) method, 10 mV amplitude AC signal was applied to the specimen electrode at OCP in the frequency range, 10 kHz to 0.01 Hz. The recording of the impedance plots was done.

2.2. Surface study of the specimen

The surface study was performed by immersing the specimen separately in 0.5M HCl and 0.5M HCl containing 1mM 2-ABT for three h. The surface image of the corroded and inhibited AA-SiC composite specimen was recorded using scanning electron microscope EVO 18-5-57. The surface roughness of these samples was recorded using the IB342 Innova model atomic force microscope.

2.3. Molecular modelling and simulation study

The quantum chemical simulation studies based on DFT (density functional theory) were performed with the help of a Schrodinger material science suite with a 6-31G^{++} basis set and B3LYP function. The molecular modelling was used to get the optimized structure of neutral, highest occupied and lowest unoccupied molecular orbitals (HOMO & LUMO) of inhibitor species in the aqueous acid medium. The quantum chemical parameters calculated were the energy of HOMO and LUMO, the energy gap, the global hardness and softness, the fraction of electron transfer, and electrophilicity.

3. Results and discussion

3.1. PDP easurements

Tafel plots or AA-SiC composite specimen immersed in 0.5M HCl and inhbited medium depicted in "Figure 2". I_{corr} (corrosion current density, μA cm^{-2}) and E_{corr} (corrosion potential, V) values were obtained from the recorded plots. The corrosion rate (CR), inhibition efficiency (IE) and surface coverage (Θ) values were computed from "Eq. (1-3)" (Fontana, 1987).

$$CR\ (mmy^{-1}) = \frac{3270 \times EW \times i_{corr}}{d} \tag{1}$$

3270 is the unit conversion constant, 'EW' denotes equivalent weight, and 'd' the density of the specimen metal (g cm^{-3}).

$$IE(\%) = \frac{i_{corr} - i_{corr(inh)}}{i_{corr}} \times 100 \tag{2}$$

$$\theta = \frac{IE(\%)}{100} \tag{3}$$

$I_{corr\ (inh)}$ represents the corrosion current density in the inhibited medium (Fontana, 1987).

In the blank medium, the corrosion rate (CR) of the composite material increases with temperature rise because of the conductivity increase of the medium. As reported, if the shift in the value of E_{corr} in inhibited medium exceeds ±85 mV as compared to the blank medium, the inhibitor involved can be grouped as either anodic or cathodic type (Li et al., 2008). "Table 1" reveals that the highest shift in E_{corr} in the inhibited medium is -28 mV compared to the blank medium. It shows that 2-ABT acts as a mixed inhibitor having more control on reactions at the cathode.
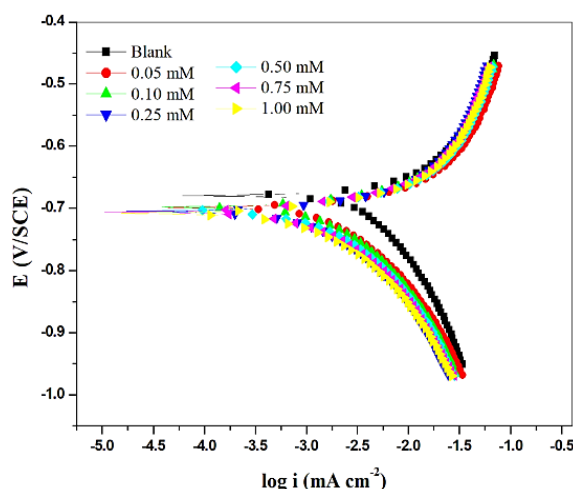

Figure 2. Tafel plots for AA-SiC composite immersed in the acid and inhibited acid medium at varying 2-ABT concentrations.

Table 1. PDP result for AA-SiC composite immersed in the acid and inhibited acid medium at varying 2-ABT concentrations and temperatures.

T (K)	Conc (mM)	E_{corr} (V)	$-\beta_c$ (mV/dec)	β_a (mV/dec)	i_{corr} (mA/cm^2)	CR (mmy^{-1})	IE (%)
303	Blank	-0.680	4.979	4.769	10.895	120.7	-
	0.05	-0.699	6.342	5.141	4.619	51.17	57.60
	0.10	-0.698	6.343	5.281	3.748	37.09	69.27
	0.25	-0.705	6.532	5.347	2.523	27.95	76.84
	0.50	-0.705	6.527	5.591	2.327	25.78	78.64
	0.75	-0.706	6.853	5.717	1.806	20.01	83.42
	1.00	-0.708	6.983	5.593	1.715	19.01	84.25
313	Blank	-0.677	4.825	4.905	14.605	162.3	-
	0.05	-0.696	5.410	4.911	7.3127	81.26	49.93
	0.10	-0.697	5.899	5.032	6.046	67.19	58.60
	0.25	-0.700	5.829	5.023	5.823	64.70	60.13
	0.50	-0.702	5.671	5.203	4.979	55.34	65.9
	0.75	-0.703	6.187	5.228	4.148	46.10	71.59
	1.00	-0.705	6.305	5.373	3.343	37.15	77.11
323	Blank	-0.708	4.864	4.909	18.46	201.9	-
	0.05	-0.703	5.406	4.912	10.70	117.0	42.03
	0.10	-0.704	5.467	4.882	9.613	105.1	47.92
	0.25	-0.704	5.662	4.684	8.172	89.37	55.73
	0.50	-0.71	5.583	5.074	7.644	83.60	58.59
	0.75	-0.71	5.651	4.898	6.492	71.00	64.83
	1.00	-0.711	5.768	5.371	6.119	66.92	66.85

As the concentration of 2-ABT increases in the acid medium, both the i_{corr} and *CR* decreases ("Table 1") drastically, indicating blocking of the composite surface due to the adsorption of 2-ABT (Khaled & Al-Qahtani, 2009). Hence the *IE* of 2-ABT increases with its concentration. On the other hand, a rise in the temperature of the medium decreases the *IE* of 2-ABT. It may be because of the desorption of already adsorbed 2-ABT molecules from the composite surface (Shetty & Kumari, 2020). As per "Table 1", the anodic slope (β_a) does not change significantly with a rise in 2-ABT concentration in the acid medium. It indicates that the added 2-ABT blocks the anodic sites without altering the inhibition mechanism, controlling the corrosion of the composite material. Similarly, the cathodic slope (β_c) values are not changing much with the rise in 2-ABT concentration. The increase in 2-ABT concentration increases the energy barrier for the proton discharge reaction and hence controls the cathodic reaction (Ahamed & Quraishi, 2009; Moretti et al., 1996).

3.2. Evaluation of kinetic parameters

The kinetic parameters like the energy of activation (E_a), enthalpy change (ΔH_a) and entropy change (ΔS_a) of activation become significant factors in deciding the adsorption type of in-

hibitor on the composite. From "Table 1", it is evident that *IE of 2-ABT* decreased with a rise in temperature, which may be due to the weaker adsorption of 2-ABT at higher temperatures, probably because of the shorter time lag between the adsorption and desorption (Shetty & Kumari, 2020). As a result, some of the adsorbed 2-ABT molecules from the composite surface may be released, exposing more surface area for the direct contact of acid, increasing *CR,* and reducing the *IE*. The inhibition efficiency decreased as the temperature of the medium increased, indicating that inhibition occurs by physisorption at higher temperatures (Abd El Rehim et al., 2002).

E_a can be calculated using the Arrhenius equation "Eq. 4" (Schorr & Yahalom, 1972).

$$\ln(CR) = B - \frac{E_a}{RT} \tag{4}$$

$$R = \frac{RT}{Nh} \exp\left(\frac{\Delta S^{\#}}{R}\right) \exp\left(\frac{-\Delta H^{\#}}{RT}\right) \tag{5}$$

'N' represents Avogadro's number, and 'h' denotes Planck's constant. "Figure 4" shows ln(CR/T) versus 1/T plot for AA-SiC composite in a 0.5 M HCl solution with varying 2-ABT concentrations. The plot slope gives ΔH_a value, and the intercept provides the ΔS_a value.
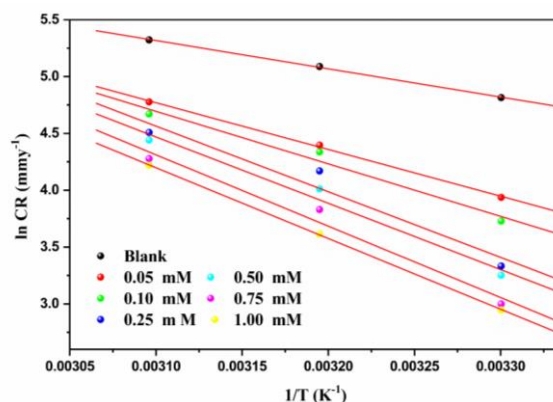

Figure 3. Arrhenius plot for AA-SiC composite in 0.5M HCl with varying 2-ABT concentrations.
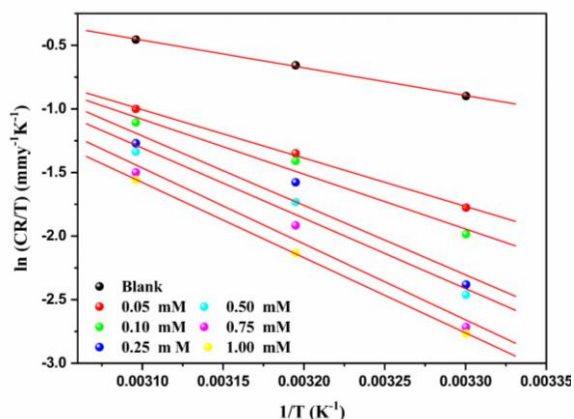

Figure 4. The plot of ln(CR/T) versus 1/T for AA-SiC composite in 0.5M HCl with varying 2- ABT concentrations.

Table 2. Kinetic parameters for AA-SiC composite in 0.5M HCl with varying 2-ABT concentrations.

C_{Inh} (mM)	E_a (kJmol^{-1})	R^2	$\Delta H^{\#}$ (kJmol^{-1})	$\Delta S^{\#}$ (Jmol^{-1}K^{-1})
Blank	20.68	0.999	18.08	-145.29
0.05	34.19	0.999	31.59	-107.93
0.10	38.42	0.989	35.82	-95.47
0.25	48.02	0.976	45.41	-66.80
0.50	48.51	0.990	45.91	-66.05
0.75	52.21	0.988	49.61	-55.89
1.00	51.76	0.999	49.15	-58.25

The kinetic parameters for AA-SiC composite in 0.5M HCl with varying 2-ABT concentrations are given in "Table 2". The results indicate that the E_a value in the inhibited medium is higher than that in the blank medium, indicating the physisorption of 2-ABT on the composite (Khaled & Al-Qahtani, 2009). Thus, the physisorption of 2-ABT molecules creates a protective barrier on the composite surface, controlling the corrosion of composite material. The ΔS_a value is negative, revealing the decrease in disorderliness occurring during the inhibition process.

3.3. Adsorption behaviour of 2-ABT
The inhibition of corrosion occurs by inhibitor adsorption on the metal. Adsorption isotherm followed reveals the nature of inhibitor interaction at the metal surface. The surface coverage values (ϑ) obtained are applied to different adsorption isotherms. The relation (Khaled & Al-Qahtani, 2009) "Eq. 6" represents the best fitment obtained with the Langmuir isotherm model.

$$\frac{C_{inh}}{\theta} = \frac{1}{K} + C_{inh} \tag{6}$$

C_{inh} represents the 2-ABT concentration (mM), and K_{ads} indicates the adsorption equilibrium constant (M^{-1}).

"Figure 5" indicates the Langmuir isotherm plot for 2-ABT adsorption on AA-SiC-composite. The straight-line plots obtained showed R^2 (correlation coefficient) values nearer to one, suggesting that Langmuir isothermal model followed for 2-ABT adsorption on the AA-SiC surface. The ΔG^0_{ads} (standard free energy of adsorption) values for the inhibitor calculated

using the values of K_{ads} given by the relation, "Eq. 7" (Bayol et al., 2007):

$$K_{ads} = \frac{1}{55.5} e(\frac{-\Delta G^{\circ}_{ads}}{RT}) \tag{7}$$

55.5 mol/dm^3 is equal to the concentration of water.

"Figure 6" depicts a straight-line obtained by plotting ΔG^0_{ads} versus T. The slope of the straight line and its intercept give the standard enthalpy change (ΔH^0_{ads}) and standard entropy change (ΔS^0_{ads}) of adsorption, respectively, according to "Eq. 8". The adsorption parameters obtained are tabulated in "Table 3".

$$\Delta G^{\circ}_{ads} = \Delta H^{\circ}_{ads} - T\Delta S^{\circ}_{ads} \tag{8}$$

"Table 3" shows the higher K_{ads} values, revealing the stable inhibitor film formation by 2-ABT on the composite surface and resulting in a higher inhibitive action (Tang et al., 2006). The ΔG^0_{ads} value is negative, which indicate that the 2-ABT adsorption is spontaneous, and a stable film of 2-ABT formed on the composite. As reported elsewhere (Kumari et al., 2017), if the $\Delta G^0_{ad} \leq -20$ kJmol^{-1}, it indicates physisorption, while the $\Delta G^0_{ads} \geq -40$ kJmol^{-1} means chemisorption of inhibitor. The ΔG^0_{ads} values for 2-ABT lie around -35 kJmol^{-1}, suggesting mixed adsorption of 2-ABT on AA-SiC composite. If the ΔH^0_{ads} value is less than -40 kJmol^{-1}, it corresponds to physisorption; if it is approaching 100 kJmol^{-1}, then it is chemisorption. In this case, ΔH^0_{ads} is negative and approaching -40 kJmol^{-1} (i.e., ΔH^0_{ads} = -37.72 kJmol^{-1}), indicating physisorption (Singh et al., 2010). The negative ΔS^0_{ads} value reveals the decrease in disorder occurring in the inhibition process.
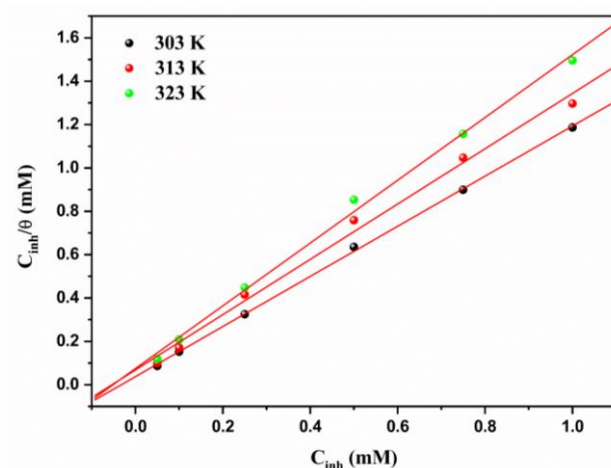
Figure 5. Langmuir´s isotherm for the 2-ABT adsorption on AA-SIC in 0.5M HCl.
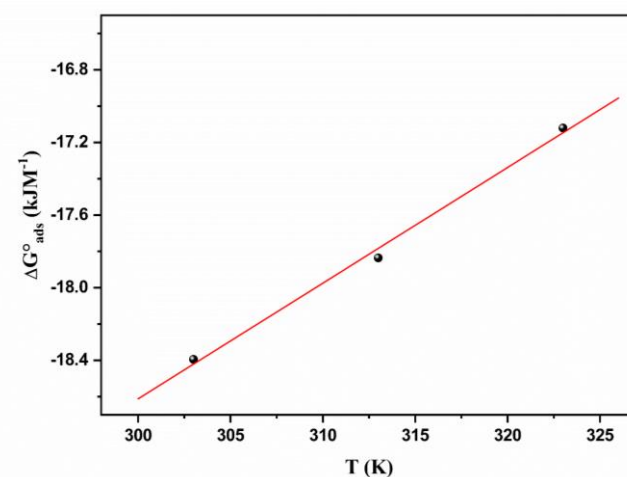
Figure 6. The plot of ΔG^0_{ads} versus T for 2-ABT adsorption on AA-SIC composite.

Table 3. The thermodynamic results for 2-ABT adsorption on AA-SiC composite.

T (K)	303	313	323
K_{ads} (M^{-1})	26724.6	14582.0	8733.01
R^2	0.999	0.996	0.998
$\Delta G°_{ads}$ (kJmol^{-1})	-35.76	-35.44	-35.12
$\Delta H°_{ads}$ (kJmol^{-1})	-45.46		
$\Delta S°_{ads}$ (Jmol^{-1}K^{-1})	-0.032		

3.4. EIS measurements

EIS studies were performed to confirm the result obtained by PDP measurements. Nyquist plots for AA-SiC composite in the blank and inhibited medium are shown in "Figure 7". It shows capacitive loops at the high-frequency and inductive loops at the low-frequency region. The plot reveals that as 2-ABT concentration increased, the semicircle diameter also increased, implying the possible reduction in corrosion rate (Nablé et al., 2021). The depressed capacitive loop observed may be related to the specimen's surface factors like inhomogeneity, roughness, corrosion product, or absorbed inhibitor (Jüttner et al., 1990). The Nyquist plot of a similar kind is reported elsewhere on the corrosion inhibition of aluminium alloys and their composites (Kumari et al., 2020; Noor, 2009; Pinto et al., 2011). The equivalent circuit was obtained by simulating the EIS results using Zsimpwin software (version 3.21). "Figure 8" depicts the simulating curve and the equivalent circuit. The equivalent circuit includes five elements: R_s (solution resistance), R_L (inductive resistance), R_{ct} (charge transfer resistance), L (inductive element), and Q (constant phase element). Q is parallel to R_{ct} and R_L, whereas L is in series with R_L.

The data from the equivalent circuit used to get the polarization resistance (R_p) as given in "Eq. 9" (Noor 2009):

$$R_p = \frac{R_{ct} \times R_L}{R_{ct} + R_L} \tag{9}$$

the double-layer capacitance (C_{dl}) values computed from "Eq. 10" (Hsu & Mansfeld, 2001):

$$C_{dl} = \frac{1}{2\pi f_{max} R_p} \tag{10}$$

f_{max} denotes the frequency where the imaginary part of the impedance is maximum.

IE (%) was computed using the polarization resistance values in the acid medium (R_p) and inhibited acid medium ($R_{p(inh)}$) as per the "Eq. 11" (Noor, 2009):

$$IE(\%) = \frac{R_{p(inh)} - R_p}{R_{p(inh)}} \times 100 \tag{11}$$

EIS results for 2-ABT are given in "Table 5". R_p value ("Table 4") increased while C_{dl} value decreased on increasing 2-ABT concentration. The increase in R_p value indicates the increase in the resistance offered for the corrosion of the composite, resulting in corrosion control (Lebrini et al., 2007). The thickness of the electrical double-layer at the metal/acid contact increases with the rise in 2-ABT concentration, causing the decrease in C_{dl} value (Bentiss et al., 2000)

Figure 7. (a) Nyquist plots for AA-SiC composite in the blank and inhibited solution at 303 K
(b) The simulating curve and equivalent circuit.

Table 4. EIS results for AA-SiC composite in the blank and inhibited medium at varying temperatures.

T (K)	C_{Inh} (mM)	R_p ($\Omega\,cm^2$)	C_{dl} ($\mu\,Fcm^{-2}$)	IE (%)
303	Blank	3.56	10019	-
	0.05	7.74	4259	54.02
	0.10	10.38	2776	65.70
	0.25	13.02	2151	72.64
	0.50	14.04	1850	74.63
	0.75	16.70	1513	78.67
	1.00	17.88	1318	80.08
313	Blank	2.68	22481	-
	0.05	5.08	10979	47.19
	0.10	5.93	9310	54.75
	0.25	6.34	8462	57.67
	0.50	7.264	7168	63.04
	0.75	8.38	5460	68.00
	1.00	9.97	4412	73.09
323	Blank	1.40	90820	-
	0.05	2.311	46219	39.28
	0.10	2.60	36694	46.04
	0.25	2.99	28692	53.07
	0.50	3.28	25378	57.33
	0.75	3.70	19887	62.16
	1.00	4.079	16856	65.59

3.5. Corrosion inhibition mechanism

In the case of AA-SiC composite in contact with an acidic medium, the aluminium metal with lower standard electrode potential (−1.66 V) acts as an anodic area. In contrast, SiC acts as a cathodic area because of its semiconductor nature. In the HCl medium, the passive film of oxide formed on the composite was destroyed, resulting in its corrosion. The deterioration of the metal can occur as per the following reactions (Bereket & Pinarbaşi, 2004).

Reactions at the anodic region:

$$Al + Cl^- \longleftrightarrow AlCl^-_{ads} \qquad (12)$$

$$AlCl^-_{ads} + Cl \longrightarrow AlCl^+_2 + 3e^- \qquad (13)$$

Reactions at the cathodic region.

$$H + e^- \longrightarrow H_{ads} \qquad (14)$$

$$H_{ads} + H_{ads} \longrightarrow H_2 \qquad (15)$$

The inhibitive action depends on inhibitor adsorption on the composite surface. According to one concept, inhibition of corrosion in an aqueous medium can take place due to the displacement of adsorbed water molecules at the metal surfa-ce by the inhibitor molecules as per the reaction (Abd El-Rehim et al., 1999):

$$Inh_{(aq)} + nH_2O \longleftrightarrow inh_{(ads)} + nH_2O_{(aq)} \qquad (16)$$
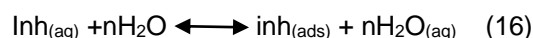
the $\Delta H°_{ads}$ and $\Delta G°_{ads}$ values suggest the physisorption of 2-ABT on the composite surface. Al metal can acquire a positive charge in contact with an acidic chloride medium since its pH_{Zch} value (i.e., pH at zero charge potential) is 9.1. Hence, in a hydrochloric acid medium, the positively charged composite surface can absorb negatively charged chloride ions.

In an acidic medium like that used in the present investigation, the protonation of the 2-ABT molecules can occur. The composite surface with a negative charge can attract protonated inhibitor, 2-ABTH$^+$ in the acid medium due to electrostatic attraction resulting in a physical barrier ("Figure 8 (a)"). Thus, this protective film can prevent direct contact of the composite material with the acid medium, controlling the deterioration of the composite. In the case of 2-ABT, the heteroatoms (N and S) and aromatic ring's π-electrons can interact with composite metal, leading to a coordinate type bond ("Figure 8 (b)"). It can result in the chemisorption of 2-ABT molecules on the composite surface. The planarity of the 2-ABT molecule can also lead to its stronger adsorption by covering the larger surface area of the composite (Yadav et al., 2015).

3.6. Analysis of SEM Images

"Figure 9(a)" represents the SEM image of AA-SiC composite dipped in 0.5M HCl. The specimen surface showed a rough surface containing more cavities. In an acid medium, galvanic corrosion can occur due to the electrical contact between cathodic SiC particles and anodic aluminium alloy matrix. SEM images of the inhibited composite specimen surface indicated a uniform surface with a few cavities, as depicted by "Figure 9(b)". The adsorption of 2-ABT blocks the detached SiC particulate zone at the composite surface. The smooth surface exposed by the inhibited Specimen may be due to the creation

of barrier film by inhibitor, leading to the corrosion protection of the composite material.

3.7. Analysis of AFM images

The AFM pictures of the composite sample immersed in blank and inhibited solutions are displayed in "Figure 10(a) & (b)". The observed surface roughness results are presented in "Table 5". It is evident from the surface roughness results that the average (R_a) and root mean square (R_q) roughness values for the inhibited specimen were much lower compared to the corroded sample, suggesting 2-ABT's adsorption on the composite.
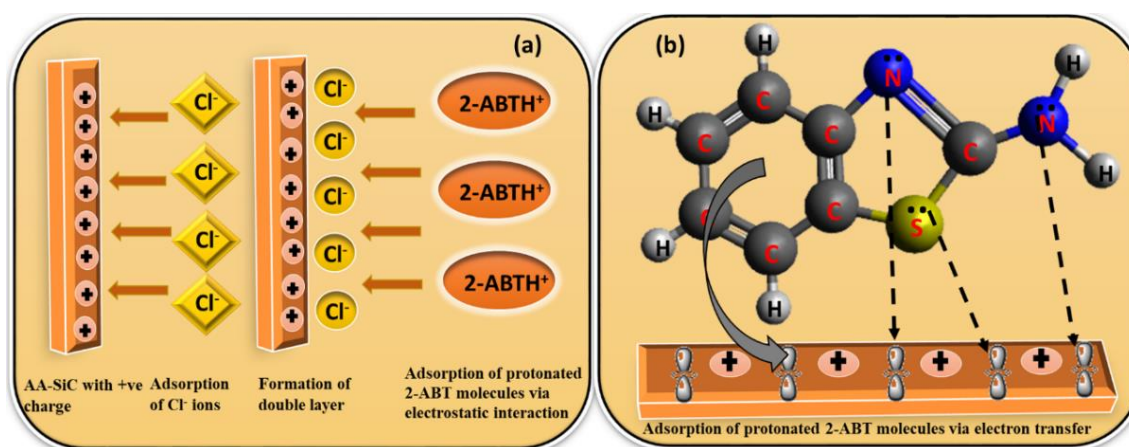
Figure 8. Pictorial representation of (a) Physisorption and
(b) Chemisorption mode for 2-ABT molecules on the composite surface.
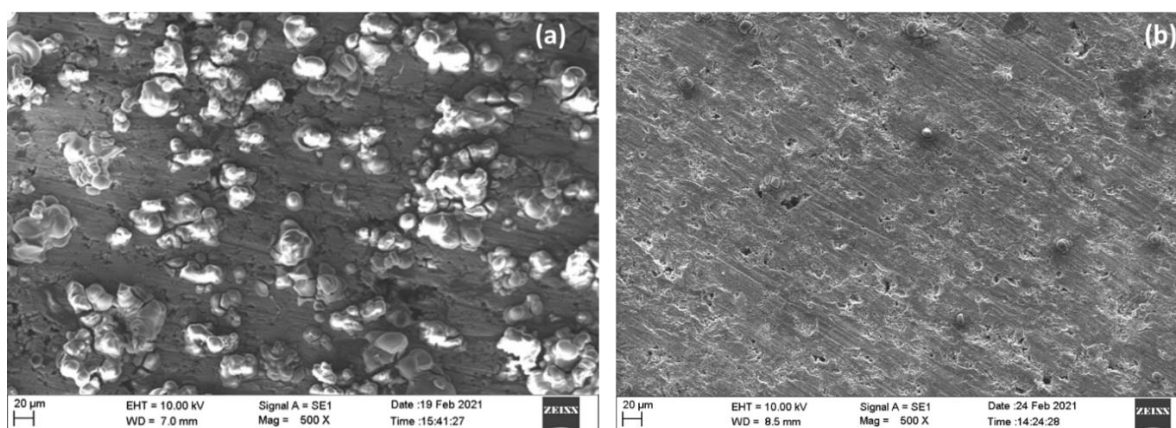
Figure 9. SEM pictures of Al-SiC composite specimen immersed in
a) 0.5M HCl, and b) (0.5M HCl + 1 mM 2-ABT).

3.7. Analysis of AFM images

The AFM pictures of the composite sample immersed in blank and inhibited solutions are displayed in "Figure 10(a) & (b)". The observed surface roughness results are presented in "Table 5". It is evident from the surface roughness results that the average (R_a) and root mean square (R_q) roughness values for the inhibited specimen were much lower compared to the corroded sample, suggesting 2-ABT's adsorption on the composite.

3.8. Quantum chemical study

Application of the quantum chemical approaches is significant for evaluating the relationship between the molecular structure of the inhibitor and its inhibition activity (Ma et al., 2006). The interaction of inhibitor molecules with the metal surface controls the extent of its adsorption and hence its inhibition performance. The inhibitor molecule's electron donating/accepting nature decides its reactivity. In this context, the quantum chemical parameters like E_{HOMO}, E_{LUMO}, and energy gap (ΔE_g) values play an essential role. The Mullikan charge on the atoms of the inhibitor molecule gives information about the active sites available for adsorption in the inhibitor molecule and their interactions with the metal surface.

The inhibitor employed in the present work can exist as tautomer (Wazzan et al., 2020), namely, amino (2-aminobenzothiazole) and imino (2-imino benzothiazole) ("Figure 11"). Since both amino and imino tautomers can coexist in a solution, the theoretical analysis of both tautomers is conducted by DFT using the 6-31G** basis set. As reported elsewhere, 2-ABT can protonate in an acidic medium at the amino nitrogen (Tay et al., 2014). The protonated form (2-ABTH⁺) can influence the inhibition process. Hence, along with amino and imino forms, the protonated form is also considered for the DFT calculations.

In 2-ABT, the heteroatoms with high negative Mullikan charges ("Figure 12") are the preferable active sites for the donor-acceptor interactions. N10 (-0.64) and N7 (-0.50) in the amino; N10 (-0.60) and N7 (-0. 56) in the imino and N10 (-0.61) and N7 (0.41) atoms in the protonated form with high negative charges probably act as the active adsorption centers. "Figure 13(a-i)" shows the optimized molecular structures of amino, imino, and protonated forms of ABT and their HOMO and LUMO orbitals. The DFT parameters were computed (Zhan et al., 2003). E_{HOMO}, E_{LUMO}, ΔE_g (energy gap), I (ionization potential), A (electron affinity), χ (electronegativity), **η** (hardness), **σ** (softness), **ω** (electrophilicity index) and **ΔN** (fraction of electron transferred) values are presented in "Table 6".
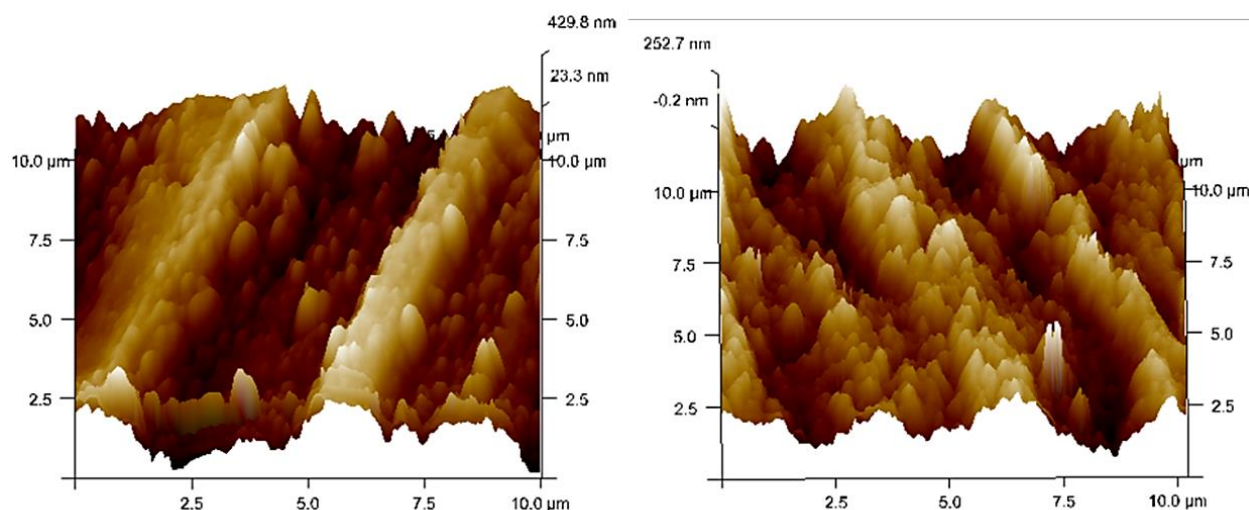

Figure 10. AFM images of AA-SiC composite specimen immersed in a) 0.5M HCl, and b) (0.5M HCl+ 1mM 2-ABT).

Table 5. AFM data for AA-SiC composite immersed in the blank and inhibited medium.

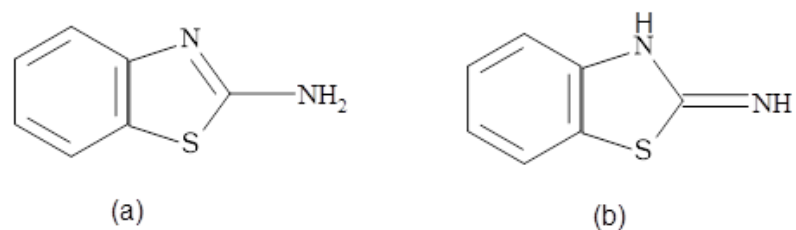| Samples	R_a (nm)	R_q (nm)
Specimen dipped in 0.5M HCl	114.0	135.0
Specimen dipped in (0.5M HCl + 1mM 2-ABT)	61.5	76.2

Figure 11. The chemical structure of (a) amino and (b) imino tautomers of 2-ABT.
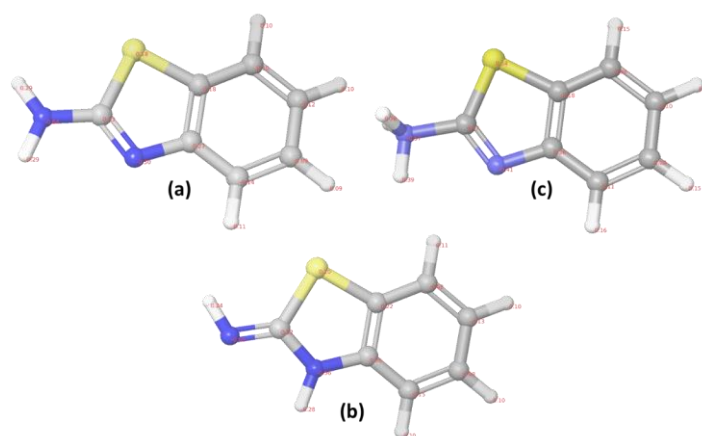

Figure 12. Mullikan charges on (a) amino, (b) imino, and (b) protonated form of 2-ABT.
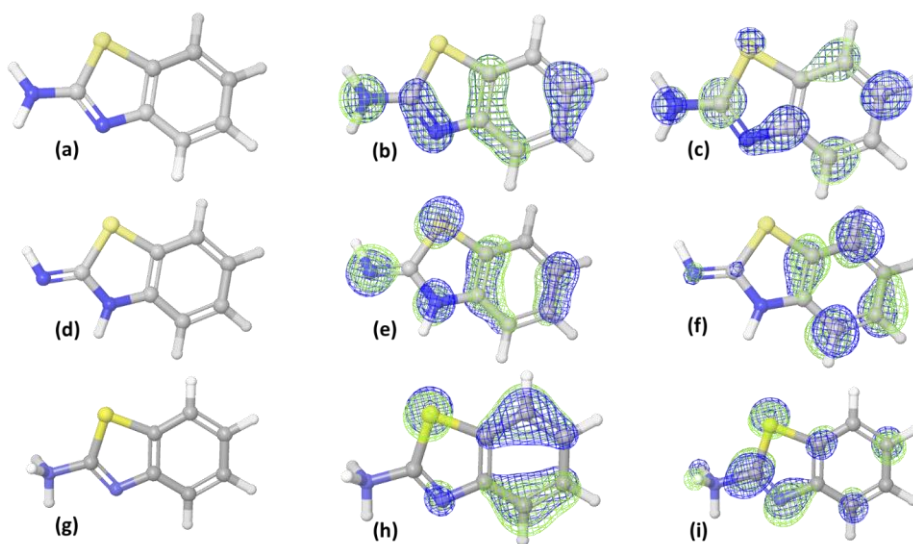

Figure 13. (a) The optimized molecular structure, (b) HOMO, and (c) LUMO of amino; (d) the optimized molecular structure, (e) HOMO, and (f) LUMO of imino; and (g) the optimized molecular structure, (h) HOMO, and (i) LUMO of protonated 2-ABT.

The E_{HOMO} and E_{LUMO} value are related to I (Ionization potential) and A (Electron affinity) values, respectively, as per the relations, "Eq. (17 -18)" (Zhan et al., 2003).

$$I = - E_{HOMO} \qquad (17)$$

$$A = - E_{LUMO} \qquad (18)$$

The χ, **η**, and **σ** values were computed using "Eq. (19-21)", respectively (Zhan et al., 2003; Pearson 1988).

$$\chi = \frac{I+A}{2} \qquad (19)$$

$$\eta = \frac{I-A}{2} \qquad (20)$$

$$\sigma = \frac{1}{\eta} \qquad (21)$$

E_{HOMO} value reflects the electron-releasing nature of an inhibitor molecule, while E_{LUMO} values show its electron accepting nature. The extent of the inhibitor's adsorption on the composite surface improves with higher E_{HOMO} and lower E_{LUMO} values. It is clear from "Table 6" that the E_{HOMO} value of imino, amino and hydrogenated forms of the inhibitor are in the order -5.547 eV **>** -5.598 eV **>**-10.282 eV. It reveals that the imino form can readily donate electrons to the Al atom's empty d-orbitals, resulting in a coordinate type bond. Similarly, the E_{LUMO} value of amino, imino, and protonated forms of the inhibitor are in the order -0.371 eV **>** -0.430 eV **>** -5.118 eV. It indicates that the protonated form (2-ABTH⁺) can readily accept electrons from the Al atom resulting in a back-donating type bond. These bonding processes help in stronger adsorption of inhibitors on the composite surface (Arslan et al., 2009).

The inhibitor molecule's energy gap (ΔE_g) plays a vital role in determining the reactivity, leading to better adsorption on the composite surface. The reactivity of the inhibitor molecule increases with decreasing ΔE_g value, leading to stronger adsorption and increasing IE (Ahamad et al., 2010). The ΔE_g value ("Table 6") exhibited by the inhibitors amino, imino and hydrogenated forms are 5.227 eV **>** 5.117 eV **>** 5.094 eV. It reveals that the protonated and imino form of the inhibitor is the most reactive and readily adsorb on the composite surface, resulting in higher inhibition performance. Therefore, the adsorption of ABT through its imino and protonated species plays a vital role in corrosion inhibition.

The hardness (**η**) and softness (**σ**) values are significant parameters in evaluating the molecular stability of the inhibitor and its reactivity. A soft molecule shows a lesser ΔE_g value while a hard molecule exhibits a high ΔE_g value. As a result, soft molecules show higher reactivity than hard ones

since they can readily donate electrons. An inhibitor molecule with a higher **σ** value and a lower **η** value shows better adsorption and good inhibitive performance (Masoud et al., 2010). From "Table 6", imino and protonated 2-ABT show the lowest ΔE_g value and hardness but the highest softness. Thus, the inhibitor could have shown good inhibitive performance in imino and protonated forms. It indicates the possibility of mixed adsorption of ABT on the composite surface, agreeing with the experimental results (ΔG^0_{ads} and ΔH^0_{ads}).

The fraction of electrons transferred (ΔN) value measures the inhibition effect caused by the inhibitor (Sastri & Perumareddi, 1997). The fraction of electrons transferred from 2-ABT molecules to the composite surface, ΔN, was computed using "Eq. 22" (Pearson, 1990).

$$\Delta N = \frac{X_{Al} - X_{Inh}}{2(\eta_{Al} + \eta_{Inh})} = \frac{\phi_{Al} - X_{Inh}}{2\,\eta_{Inh}} \qquad (22)$$

In this relation, **χ**$_{Al}$ and **χ**$_{Inh}$ denote the electronegativity, whereas **η**$_{Al}$ and **η**$_{Inh}$ represent the hardness of Al and inhibitor, respectively. The theoretical value of electronegativity (**φ**Al) in the present work is taken as 4.28 eV (Kokalj & Kovačević, 2011) and **η**$_{Al}$ as zero (Pearson, 1990). The value of ΔN **>** 0 shows the higher tendency of inhibitor molecules to donate electrons. At the same time, ΔN **<** 0 indicate a higher preference to accept electrons (Dahiya et al., 2018). The ΔN value presented in "Table 6" reveals that the inhibitor's imino (0.255) and amino (0.248) forms can readily donate. In contrast, the hydrogenated form (- 0.679) can easily accept electrons. As reported elsewhere, the value of ΔN less than 3.6 indicates that IE increases with a rise in the electron-releasing tendency of the inhibitor on the composite surface (Lukovits et al., 2001). Both amino and imino forms are the electron donors in the present inhibitor, whereas the composite metal surface is the electron acceptor.

The electrophilicity index (**ω**) indicates the electrophilic power of an inhibitor. The value of **ω** can be obtained using "Eq. 23" (Parr et al., 1999).

$$\omega = \frac{\mu^2}{2\eta} \qquad (23)$$

In this relation, μ is the electronic chemical potential, given by "Eq. 24" (Pearson, 1988).

$$-\mu = \frac{I+A}{2} = \chi \qquad (24)$$

The higher the **ω** value excellent is its ability to accept electrons (Obot & Obi-Egbedi, 2010). The protonated inhibitor shows the highest **ω** value (11.745), indicating that it readily accepts electrons from composite metal. As a result, the extent of adsorption of the inhibitor on the composite surface becomes stronger.

Table 6. The DFT parameters for amino, imino, and protonated forms of the inhibitor.

Property	Amino form	Imino form	Protonated form
E_{HOMO}	-5.598 eV	-5.547 eV	-10.282 eV
E_{LUMO}	-0.371 eV	-0.430 eV	-5.188 eV
ΔE_g	5.227 eV	5.117 eV	5.094 eV
$I = -E_{HOMO}$	5.598 eV	5.547 eV	10.282 eV
$A = -E_{LUMO}$	0.371 eV	0.430 eV	5.188 eV
$\chi = \dfrac{I+A}{2}$	2.984 eV	2.977 eV	7.735 eV
$\eta = \dfrac{I-A}{2}$	2.613 eV	2.558 eV	2.547 eV
$\sigma = \dfrac{1}{\eta}$	0.383 eV	0.391 eV	0.393 eV
ω	1.704	1.732	11.745
ΔN	0.248	0.255	-0.679

4. Conclusions

Based on the experimental and theoretical investigations, the following conclusions were drawn:

1. 2-ABT can be a potential corrosion inhibitor for AA-SiC composite

2. Inhibition performance found to improve on increasing 2-ABT concentration and decrease on rising temperature of the medium

3. 2-ABT showed mixed inhibitor behaviour having more control on cathodic reaction. It underwent physisorption and obeyed the isotherm model of Langmuir's

4. Surface analysis using SEM and AFM pictures confirmed the 2-ABT adsorption on the composite

5. The PDP results are in line with the results of EIS

6. The experimental results were validated by theoretical calculations using DFT

Conflict of interest

The authors have no competing interests to declare relevant to this article's content.

Acknowledgements

Funding

References

Abd El Rehim, S. S., Hassan, H. H., & Amin, M. A. (2002). The corrosion inhibition study of sodium dodecyl benzene sulphonate to aluminium and its alloys in 1.0 M HCl solution. *Materials Chemistry and Physics, 78*(2), 337-348. https://doi.org/10.1016/S0254-0584(01)00602-2

El-Rehim, S. A., Ibrahim, M. A., & Khaled, K. F. (1999). 4-Aminoantipyrine as an inhibitor of mild steel corrosion in HCl solution. *Journal of Applied Electrochemistry, 29*, 593-599. https://doi.org/10.1023/A:1003450818083

Ahamad, I., Prasad, R., & Quraishi, M. A. (2010). Experimental and quantum chemical characterization of the adsorption of some Schiff base compounds of phthaloyl thiocarbohydrazide on the mild steel in acid solutions. *Materials Chemistry and Physics, 124*(2-3), 1155-1165. https://doi.org/10.1016/j.matchemphys.2010.08.051

Ahamad, I., & Quraishi, M. A. (2009). Bis (benzimidazol-2-yl) disulphide: an efficient water soluble inhibitor for corrosion of mild steel in acid media. *Corrosion science, 51*(9), 2006-2013. https://doi.org/10.1016/j.corsci.2009.05.026

Arslan, T., Kandemirli, F., Ebenso, E. E., Love, I., & Alemu, H. (2009). Quantum chemical studies on the corrosion inhibition of some sulphonamides on mild steel in acidic medium. *Corrosion Science, 51*(1), 35-47. https://doi.org/10.1016/j.corsci.2008.10.016

Bayol, E., Kayakırılmaz, K., & Erbil, M. (2007). The inhibitive effect of hexamethylenetetramine on the acid corrosion of steel. *Materials Chemistry and Physics, 104*(1), 74-82. https://doi.org/10.1016/j.matchemphys.2007.02.073

Bentiss, F., Traisnel, M., & Lagrenee, M. (2000). The substituted 1, 3, 4-oxadiazoles: a new class of corrosion inhibitors of mild steel in acidic media. *Corrosion science, 42*(1), 127-146. https://doi.org/10.1016/S0010-938X(99)00049-9

Bereket, G., & Pinarbaşi, A. (2004). Electrochemical thermodynamic and kinetic studies of the behaviour of aluminium in hydrochloric acid containing various benzotriazole derivatives. *Corrosion engineering, science and technology, 39*(4), 308-312. https://doi.org/10.1179/174327804X13136

Bobic, B., Mitrovic, S., Babic, M., & Bobic, I. (2010). Corrosion of metal-matrix composites with aluminium alloy substrate. *Tribology in industry*. 32(1), 3-11.

Dahiya, S., Saini, N., Dahiya, N., Lgaz, H., Salghi, R., Jodeh, S., & Lata, S. (2018). Corrosion inhibition activity of an expired antibacterial drug in acidic media amid elucidate DFT and MD simulations. *Portugaliae Electrochimica Acta, 36*(3), 213-230. https://doi.org/10.4152/pea.201803213

Danaee, I., Gholami, M., RashvandAvei, M., & Maddahy, M. H. (2015). Quantum chemical and experimental investigations on inhibitory behavior of amino–imino tautomeric equilibrium of 2-aminobenzothiazole on steel corrosion in H2SO4 solution. *Journal of Industrial and Engineering Chemistry, 26*, 81-94. https://doi.org/10.1016/j.jiec.2014.11.018

Fontana, M. G. (1987). Corrosion Engineering, Singapore: McGraw-Hill, 1987, pp. 3-10.

Hsu, C. H., & Mansfeld, F. (2001). Concerning the conversion of the constant phase element parameter Y0 into a capacitance. *Corrosion, 57*(09). https://doi.org/10.5006/1.3280607

Jafari, H., Akbarzade, K., & Danaee, I. (2019). Corrosion inhibition of carbon steel immersed in a 1 M HCl solution using benzothiazole derivatives. *Arabian journal of chemistry, 12*(7), 1387-1394. https://doi.org/10.1016/j.arabjc.2014.11.018

Jüttner, K. (1990). Electrochemical impedance spectroscopy (EIS) of corrosion processes on inhomogeneous surfaces. *Electrochimica Acta, 35*(10), 1501-1508. https://doi.org/10.1016/0013-4686(90)80004-8

Khaled, K. F., & Al-Qahtani, M. M. (2009). The inhibitive effect of some tetrazole derivatives towards Al corrosion in acid solution: Chemical, electrochemical and theoretical studies. *Materials Chemistry and Physics, 113*(1), 150-158. https://doi.org/10.1016/j.matchemphys.2008.07.060

Koch, G., Vamey, J., Thompson, N., Moghissi, O., Gould, M. & Payer, J. (2016). International measures of prevention, application, and economics of corrosion technologies study, Houston, TX: NACE International, pp. 1 - 4.

Kokalj, A., & Kovačević, N. (2011). On the consistent use of electrophilicity index and HSAB-based electron transfer and its associated change of energy parameters. *Chemical Physics Letters, 507*(1-3), 181-184. https://doi.org/10.1016/j.cplett.2011.03.045

Kumari, P. P., Shetty, P., & Sunil, D. (2020). Effect of cysteine as environmentally friendly inhibitor on AA6061-T6 corrosion in 0.5 M HCl: electrochemical and surface studies. *Surface Engineering and Applied Electrochemistry*, *56*(5), 624-634. https://doi.org/10.3103/S1068375520050087

Kumari, P., Shetty, P., Rao, S. A., & Sunil, D. (2017). Inhibition behaviour of 2-[(2-methylquinolin-8-yl) oxy] acetohydrazide on the corrosion of mild steel in hydrochloric acid solution. *Transactions of the Indian Institute of Metals*, *70*, 1139-1150. https://doi.org/10.1007/s12666-016-0901-0

Lebrini, M., Lagrenée, M., Vezin, H., Traisnel, M., & Bentiss, F. (2007). Experimental and theoretical study for corrosion inhibition of mild steel in normal hydrochloric acid solution by some new macrocyclic polyether compounds. *Corrosion Science*, *49*(5), 2254-2269. https://doi.org/10.1016/j.corsci.2006.10.029

Li, W. H., He, Q., Zhang, S. T., Pei, C. L., & Hou, B. R. (2008). Some new triazole derivatives as inhibitors for mild steel corrosion in acidic medium. *Journal of Applied Electrochemistry*, *38*, 289-295. https://doi.org/10.1007/s10800-007-9437-7

Lukovits, I., Kalman, E., & Zucchi, F. (2001). Corrosion inhibitors—correlation between electronic structure and efficiency. *Corrosion*, *57*(1), 3-8. https://doi.org/10.5006/1.3290328

Ma, H., Chen, S., Liu, Z., & Sun, Y. (2006). Theoretical elucidation on the inhibition mechanism of pyridine–pyrazole compound: a Hartree Fock study. *Journal of Molecular Structure: THEOCHEM*, *774*(1-3), 19-22. https://doi.org/10.1016/j.theochem.2006.06.044

Masoud, M. S., Awad, M. K., Shaker, M. A., & El-Tahawy, M. M. T. (2010). The role of structural chemistry in the inhibitive performance of some aminopyrimidines on the corrosion of steel. *Corrosion Science*, *52*(7), 2387-2396. https://doi.org/10.1016/j.corsci.2010.04.011

Moretti, G., Quartarone, G., Tassan, A., & Zlngales, A. (1996). 5-Amino-and 5-chloro-indole as mild steel corrosion inhibitors in 1 N sulphuric acid. *Electrochimica Acta*, *41*(13), 1971-1980. https://doi.org/10.1016/0013-4686(95)00485-8

Nahlé, A., Salim, R., El Hajjaji, F., Aouad, M. R., Messali, M., Ech-Chihbi, E., ... & Taleb, M. (2021). Novel triazole derivatives as ecological corrosion inhibitors for mild steel in 1.0 M HCl: experimental & theoretical approach. *RSC advances*, *11*(7), 4147-4162.

Noor, E. A. (2009). Evaluation of inhibitive action of some quaternary N-heterocyclic compounds on the corrosion of Al–Cu alloy in hydrochloric acid. *Materials Chemistry and Physics*, *114*(2-3), 533-541. https://doi.org/10.1016/j.matchemphys.2008.09.065

Obot, I. B., & Obi-Egbedi, N. O. (2010). Theoretical study of benzimidazole and its derivatives and their potential activity as corrosion inhibitors. *Corrosion Science*, *52*(2), 657-660. https://doi.org/10.1016/j.corsci.2009.10.017

Parr, R. G., Szentpály, L. V., & Liu, S. (1999). Electrophilicity index. *Journal of the American Chemical Society*, *121*(9), 1922-1924.

Pearson, R. G. (1988). Absolute electronegativity and hardness: application to inorganic chemistry. *Inorganic chemistry*, *27*(4), 734-740. https://doi.org/10.1021/ic00277a030

Pearson, R. G. (1990). Hard and soft acids and bases—the evolution of a chemical concept. *Coordination chemistry reviews*, *100*, 403-425. https://doi.org/10.1016/0010-8545(90)85016-L

Pinto, G. M., Nayak, J., & Shetty, A. N. (2011). Corrosion inhibition of 6061 Al–15 vol. pct. SiC (p) composite and its base alloy in a mixture of sulphuric acid and hydrochloric acid by 4-(N, N-dimethyl amino) benzaldehyde thiosemicarbazone. *Materials Chemistry and Physics*, *125*(3), 628-640. https://doi.org/10.1016/j.matchemphys.2010.10.006

Quraishi, M. A., Wajid Khan, M. A., Ajmal, M., Muralidharan, S., & Venkatakrishna Iyer, S. (1996). Influence of substituted benzothiazoles on corrosion in acid solution. *Journal of applied electrochemistry*, *26*, 1253-1258. https://doi.org/10.1007/BF00249927

Revie, R. W., & Uhlig, H. H. (2008). *Corrosion and corrosion control: an introduction to corrosion science and engineering*. John Wiley & Sons.

Rohatgi, P.K. (1993), Metal matrix composites. Defence Sci. J. 43, 323-349.

Sanyal, B. (1981). Organic compounds as corrosion inhibitors in different environments—a review. *Progress in Organic Coatings*, *9*(2), 165-236. https://doi.org/10.1016/0033-0655(81)80009-X

Sastri, V. S., & Perumareddi, J. R. (1997). Molecular orbital theoretical studies of some organic corrosion inhibitors. *Corrosion*, *53*(08). 617-622.

Sharma, A., Triloki, Kumar, S., & Acharya, V., (2022). Basics of Metal Matrix Composites and Their Application in Transistor Electronics, in Bansal, S. A., Khanna, V., and Gupta, P. (Eds.) Metal Matrix Composites: Properties and Applications (Vol. 2) (1st ed.). NY: CRC Press. pp. 181-200. https://doi.org/10.1201/9781003194910

Schorr, M., & Yahalom, J. (1972). The significance of the energy of activation for the dissolution reaction of metal in acids. *12*(11), 867-868. https://doi.org/10.1016/S0010-938X(72)80015-5

Shetty, P. (2018). Hydrazide derivatives: an overview of their inhibition activity against acid corrosion of mild steel. *South African Journal of Chemistry*, *71*, 46-50.

Shetty, P., & Kumari, P. P. (2020). Inhibitive action of glutathione reduced on the deterioration of AA6061 in 0.5 M HCl. *Tribology in Industry*, *42*(2), 214-224. https://doi.org/10.24874/ti.785.10.19.02

Singla, M., Dwivedi, D. D., Singh, L., & Chawla, V. (2009). Development of aluminium based silicon carbide particulate metal matrix composite. *Journal of Minerals and Materials Characterization and Engineering*, *8*(06), 455.

Singh, A. K., & Quraishi, M. A. (2010). Inhibitive effect of diethylcarbamazine on the corrosion of mild steel in hydrochloric acid. *Corrosion science*, *52*(4), 1529-1535. https://doi.org/10.1016/j.corsci.2009.12.011

Tang, L., Li, X., Si, Y., Mu, G., & Liu, G. (2006). The synergistic inhibition between 8-hydroxyquinoline and chloride ion for the corrosion of cold rolled steel in 0.5 M sulfuric acid. *Materials chemistry and physics*, *95*(1), 29-38. https://doi.org/10.1016/j.matchemphys.2005.03.064

Tay, F., Duran, M., & Demirayak, Ş. (2014). A quantum chemical DFT/HF study on acidity constants of some benzothiazole and thiazole derivatives. https://doi.org/10.1039/C6RA11818F

Wazzan, N., Safi, Z., Al-Barakati, R., Al-Qurashi1, O., & Al-Khateeb, L. (2020). DFT investigation on the intramolecular and intermolecular proton transfer processes in 2-aminobenzothiazole (ABT) in the gas phase and in different solvents, *Struct Chem 31*, 243–252. https://doi.org/10.1007/s11224-019-01395-w

Xhanari, K., & Finšgar, M. (2016). Organic corrosion inhibitors for aluminium and its alloys in acid solutions: a review. *RSC advances*, *6*(67), 62833-62857. https://doi.org/10.1039/C6RA11818F

Yadav, M., Sinha, R. R., Kumar, S., & Sarkar, T. K. (2015). Corrosion inhibition effect of spiropyrimidinethiones on mild steel in 15% HCl solution: insight from electrochemical and quantum studies. *RSC advances*, *5*(87), 70832-70848. https://doi.org/10.1039/C5RA14406J

Zhan, C. G., Nichols, J. A., & Dixon, D. A. (2003). Ionization potential, electron affinity, electronegativity, hardness, and electron excitation energy: molecular properties from density functional theory orbital energies. *The Journal of Physical Chemistry A*, *107*(20), 4184-4195. https://doi.org/10.1021/jp0225774

Navya Prabhu, Prakasha Shetty, Preethi Kumari,
Sneha Kagatikar

Inhibitive action of 2-aminobezothiazole on the deterioration of AA6061-SiC composite in 0.5M HCl medium: Experimental and theoretical analysis